1974

A contribution to the study of imaging with scattered thermal neutrons.

Johannesmeyer, Charles Alan.

Pennsylvania State University

A CONTRIBUTION TO THE STUDY OF IMAGING WITH SCATTERED THERMAL NEUTRONS

Charles Alan Johannesmeyer

The Pennsylvania State University

The Graduate School

Department of Nuclear Engineering

A Contribution to the Study of Imaging With Scattered Thermal Neutrons

A Thesis in

Nuclear Engineering

by

Charles Alan Johannesmeyer

Submitted in Partial Fulfillment
of the Requirements
for the Degree of

Master of Science

November 1974

Date of Signature:

ACKNOWLEDGMENTS

The author wishes to express his sincere appreciation to Dr. Alan M. Jacobs for his professional assistance and personal encouragement during the preparation of this work. The author also wishes to thank Paul J. Rose for his assistance in providing the apparatus used for data collection.

This work and the author's course of study have been made possible through the U.S. Naval Postgraduate Education Program.

TABLE OF CONTENTS

LIST OF FIGURES

ABSTRACT

Recent developments in pseudo-holography provide the means to generate a three-dimensional image of an object from any radiation it scatters. One promising technique uses scattered radiation to cast shadows of a Fresnel zone plate, referred to as the coded image, which are recorded on film. The coded image is then decoded by passing coherent light through it which is diffracted producing an image of the radiation source.

In this paper, a brief illustration of pseudo-holography using scattered thermal neutrons is presented, along with a development of a general expression for the coded image. The remainder of the paper is devoted to developing a scattered neutron flux source function by diffusion theory methods for a non-reentrant, steady state, homogeneous body of simple geometry. To test the accuracy of the source function, the computed scattered flux is compared with some measured values. The comparison supports the diffusion approximation for detection methods which do not have a strong forward detecting preference.

I. INTRODUCTION

Recent developments in pseudo-holography provide the means to generate a three-dimensional image of an object from any radiation it scatters. One promising pseudo-holographic technique is basically a two-step process. The scattered radiation is used to cast shadows of a Fresnel zone plate (hereafter termed the coded image) which are recorded on film. The coded image is then decoded by passing coherent light through it which is diffracted producing an image of the radiation scattering source. This technique, first proposed for radiation sources by Mertz and Young[1] in x-ray astronomy, and extended to gamma ray sources by Barrett[2,3,4,5] and Rogers[6], has been successfully applied to actual image formation using x-rays scattered from an object by Sider, et al.[7] The use of scattered neutrons in image formation is presently under study by Rose, et al.[8] and provides the motivation for this paper.

The pseudo-holographic technique using scattered neutrons differs from the use of scattered x-rays only in that the film and Fresnel zone plate respond to neutrons, not x-rays, in forming the coded image. It follows that an analytical representation of the coded image can be developed by describing the scattered neutron flux, modifying the scattered flux with a Fresnel zone plate response, and applying a film (detector) response function to the modified flux (shadows) seen by the film. The first step in this analysis is an accurate description of the uninterrupted scattered flux. It is the intent of this paper to develop an analytical method which describes scattered neutron fluxes emerging from objects in a beam of thermal neutrons.

First, a brief illustration of pseudo-holography is presented along with a development of a general expression for the coded image. The remainder of the paper is devoted to developing a scattered flux source function by diffusion theory methods for a non-reentrant, steady state, homogeneous body of simple geometry. To test the accuracy of the source function the computed scattered flux is compared with some measured values.

II. BACKGROUND

A. Concept Illustration

The basic concept of the pseudo-holographic technique noted above, as applied to thermal neutrons, is illustrated in Figure 1. A Fresnel zone plate is positioned relative to the scattering body and a suitable film-converter camera as shown. The zone plate has a series of equi-area annular zones which are alternately transparent and opaque to thermal neutrons and consist, for example, of aluminum and cadmium, respectively. Considering only a point scattering source of thermal neutrons, the display on the emulsion film (the coded image) is a shadow of the zone plate the shape and size of which depend monotonically on the position of the source in the z-plane, (x,y); the position of the zone plate relative to the source plane, z_1-z; and the position of the camera relative to the zone plate, z_2-z_1. When a beam of coherent light passes through the coded image, the light is diffracted into a focal spot which is an image of the original point scatterer. Considering any object to be a set of point scatterers, any specimen can be imaged. Each plane in the object will have a different focal plane when imaged, so that the three-dimensional information in the coded image can be viewed tomographically.

B. Coded Image

Neglecting the detector resolution*, assuming a linear film response, and noting the film output is different transparencies for

*The detector resolution is idealized by considering the film and converter to be in the same plane and neglecting the film resolution.

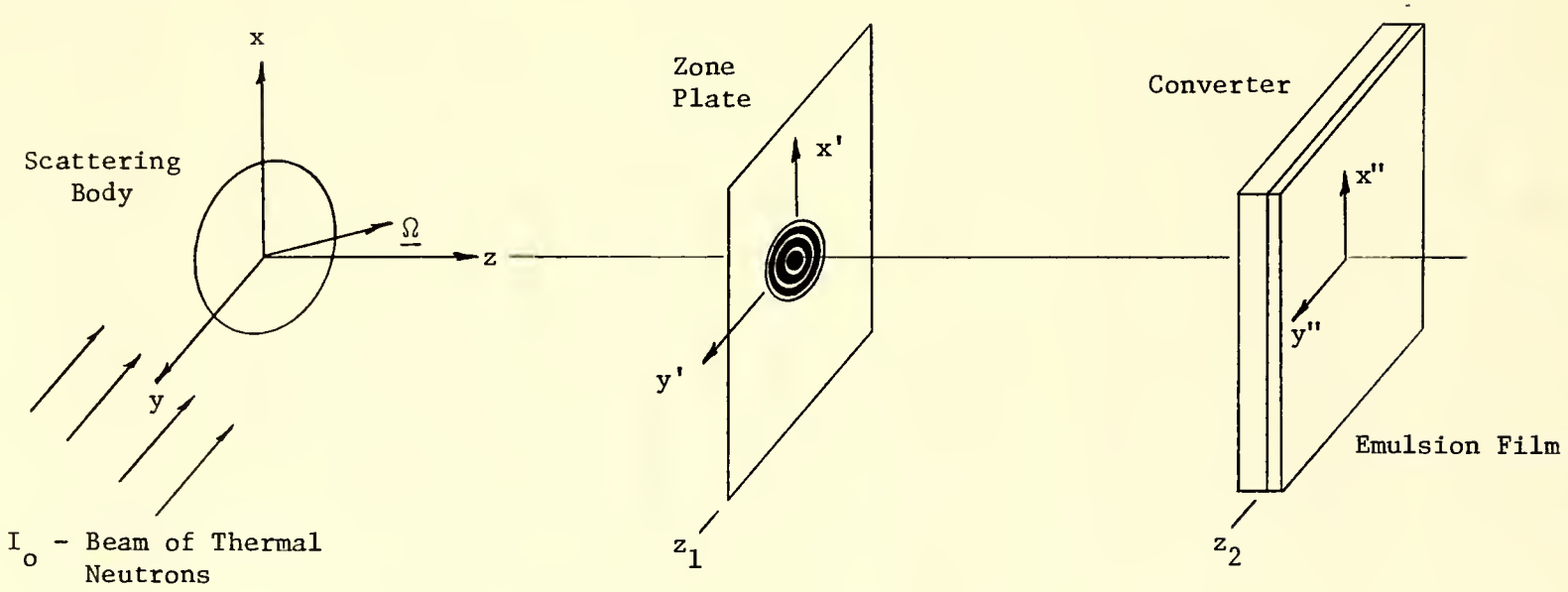

Figure 1. Scheme for Pseudo-Hologram Formation

points on the film, the coded image can be represented by the neutron flux shape in the x"y"-plane. As shown in Figure 1, (x",y") describes points in the film-converter plane at $z = z_2$; (x',y') describes points in the zone plate plane at $z = z_1$; and (x,y,z) describes points in the scattering body.

Let $F_s(x,y,z,\underline{\Omega})$, the scattering rate density, represent the number of neutrons per unit time per unit volume per solid angle scattered in the volume dxdydz about x,y,z and in the direction $d\underline{\Omega}$ about $\underline{\Omega}$. Let $G(x,y,z,\underline{\Omega} \rightarrow x",y",z_2,\underline{\Omega}")$ represent the angular flux Green's function to the film-converter plane, then

$$G(x,y,z,\underline{\Omega} \rightarrow x",y",z_2,\underline{\Omega}") = \frac{e^{-\eta(\underline{r},\underline{r}")}}{|\underline{r}-\underline{r}"|^2} \delta\left[\underline{\Omega} - \frac{\underline{r}"-\underline{r}}{|\underline{r}-\underline{r}"|}\right] \delta(\underline{\Omega}"-\underline{\Omega}) \qquad (1)$$

where $\underline{r},\underline{r}'$ and $\underline{r}"$ are vectors from the origin (see Figure 1) to points in the scattering body (x,y,z), to points in the zone plate plane (x',y',z'), and to points in the film-converter plane $(x",y",z_2)$, respectively; and $\eta(\underline{r},\underline{r}")$ is the "optical path length" between $\underline{r}$ and $\underline{r}"$.

In this case it is convenient to consider $\eta(\underline{r},\underline{r}")$ in two parts, the "optical path length" in the scattering body, $\eta_1(\underline{r},\underline{r}")$, and the "optical path length" outside the body, $\eta_2(\underline{r},\underline{r}")$. Then

$$e^{-\eta(\underline{r},\underline{r}")} = e^{-\eta_1(\underline{r},\underline{r}")} \cdot e^{-\eta_2(\underline{r},\underline{r}")} \qquad (2)$$

where the second exponential on the right hand side represents the zone plate transparency which is defined by a set of step functions or a series expansion[9].

The neutron flux, $\Phi(x'',y'',z_2)$, at the film-converter plane is then

(3)

$$\Phi(x'',y'',z_2)= \int_{\underline{\Omega}} \int_{\underline{\Omega}''} \int_{Vol} F_s(x,y,z,\underline{\Omega})G(x,y,z,\underline{\Omega} \rightarrow x'',y'',z_2,\underline{\Omega}'')d\underline{\Omega}d\underline{\Omega}''d\underline{r}$$

If an angular emitted neutron current from the surface of the body can be described as $K_s(x,y,z,\underline{\Omega})$, then

(4)

$$\Phi(x'',y'',z_2)= \int_{\underline{\Omega}} \int_{\underline{\Omega}''} \int_{S} K_s(x,y,z,\underline{\Omega})G(x,y,z,\underline{\Omega} \rightarrow x'',y'',z_2,\underline{\Omega}'')d\underline{\Omega}d\underline{\Omega}''d\underline{r}_s$$

where $\int_s$ represents integration over the body surface, $d\underline{r}_s$ is a surface element of the body and in this case $\eta_1(\underline{r},\underline{r}'') = 0$. Note that with the zone plate removed, $\eta_2(\underline{r},\underline{r}'') = 0$ in equations (3) and (4) above, and the uninterrupted scattered neutron flux at (x'',y'') in the film-converter plane is described.

To evaluate equations (3) or (4) an expression for the emitted neutron current or the scattered neutron source must be developed via a suitable neutron transport approximation. The accuracy of the source function can be verified by computing the uninterrupted scattered flux from equations (3) or (4) and comparing its shape with measured values. As noted above, the flux shape in the (x'',y'') plane is sufficient to represent the coded image.

III. SCATTERED FLUX FROM A REGULAR SOLID

For the development of a coded image of the interior structure to be practicable, the thermal neutron scattering cross section, $\bar{\Sigma}_s$, of the scattering object must be much greater than the thermal neutron absorption cross section, $\bar{\Sigma}_a$. This suggests the possible application of the diffusion approximation to neutron transport in developing a scattered source function as used in equations (3) or (4), where some approximation will be required to define the directional dependence of the scattered source function.

A. Scattered Source Function

It is assumed that an adequate test case is to examine the scattered flux from a regular solid in a beam of thermal neutrons of intensity I_o (neutrons per unit time per unit area) as shown in Figure 2, where the composition of the solid is homogeneous and such that $\bar{\Sigma}_s >> \bar{\Sigma}_a$. As mentioned earlier, either a scattering source function or an angular emitted current source function can be used in computing the scattered flux. To develop a scattering source function, the flux in the solid, $\Phi(x,y,z)$, is derived by diffusion theory methods, and the solid is considered an isotropic volumetric source of strength $\frac{\bar{\Sigma}_s \Phi(x,y,z)}{4\pi}$. The scattered flux at some point away from the solid, (x_o,y_o,z_o) in Figure 2 would be the uncollided contribution from each point in the solid. An angular emitted current source function on the surface of the solid is defined directly from the emitted current derived via diffusion theory, where some emission angular dependence

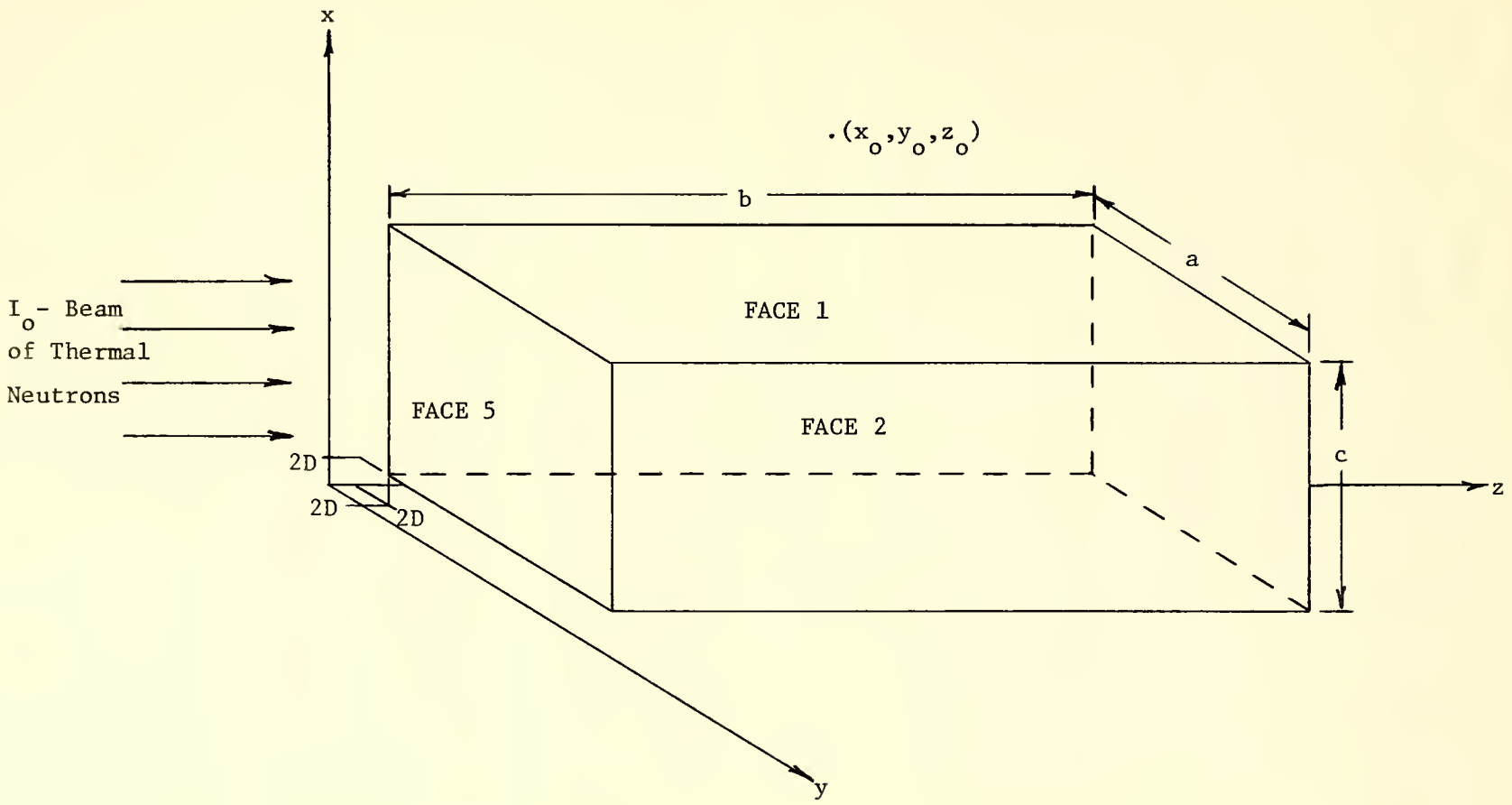

Figure 2. Test Case Geometry Used in Determining the Scattered Flux

must be assumed. The use of diffusion theory in computing reflection coefficients and the relative ease in computing the scattered flux from an angular emitted current source suggests the use of the angular emitted source.

The diffusion equation to be solved is

$$D\nabla^2\Phi(x,y,z) - \bar{\Sigma}_a\Phi(x,y,z) + S(x,y,z) = 0 \tag{5}$$

where D is the diffusion coefficient of the solid and S(x,y,z) is an isotropic volumetric source. It is convenient, in terms of describing suitable boundary conditions, to let S(x,y,z) represent the first collision scattering density, i.e.,

$$S(x,y,z) = \bar{\Sigma}_s I_o \, e^{-\bar{\Sigma}_t z} \tag{6}$$

where $\bar{\Sigma}_t$ is the total thermal neutron cross section of the solid and it is assumed that the first collision scattering density is isotropic. The boundary conditions are that $\Phi(x,y,z)$ is zero at the extrapolated boundaries of the solid.

The solution to equation (5) (see Appendix A) obtained by the method of eigenfunctions for the geometry in Figure 2 is

$$\Phi(x,y,z) = \sum_{lmn} A_{lmn} \sin\left[\frac{l\pi x}{\tilde{c}}\right] \sin\left[\frac{m\pi y}{\tilde{a}}\right] \sin\left[\frac{n\pi z}{\tilde{b}}\right] \tag{7}$$

where

$$A_{lmn} = \frac{32\ \bar{\Sigma}_s I_o K}{\bar{\Sigma}_a (1+L^2 B_{lmn}^2)\ \tilde{b} lm\pi^2 \left[\bar{\Sigma}_t^2 + \left[\frac{n\pi}{\tilde{b}}\right]\right]^2}$$

$$K = e^{-\bar{\Sigma}_t b}\left[-\bar{\Sigma}_t \sin\left[\frac{\pi n(\tilde{b}-2D)}{\tilde{b}}\right] - \frac{n\pi}{\tilde{b}} \cos\left[\frac{n\pi(\tilde{b}-2D)}{\tilde{b}}\right]\right]$$

$$+ \bar{\Sigma}_t \sin\left[\frac{n\pi 2D}{\tilde{b}}\right] + \frac{n\pi}{\tilde{b}} \cos\left[\frac{n\pi 2D}{\tilde{b}}\right]$$

$$L = D/\bar{\Sigma}_a,\ \tilde{b} = b+4D,\ \tilde{c} = c+4D,\ \tilde{a} = a+4D$$

$$B_{lmn}^2 = \left[\frac{l\pi}{\tilde{c}}\right]^2 + \left[\frac{m\pi}{\tilde{a}}\right]^2 + \left[\frac{n\pi}{\tilde{b}}\right]^2$$

Noting the symmetry in Figure 2, $x = \tilde{c}/2$ and $y = \tilde{a}/2$ is the center of symmetry in the xy-plane, and considering points (x_o, y_o, z_o) which do not see the ends of the solid, i.e., $2D<z_o<b+2D$, then the emitted current need only be defined for faces 1 and 2 of the solid. The emitted current from face 1, $J_x^+(c+2D,y,z)$, by Fick's Law is

$$J_x^+(c+2D,y,z) = \frac{\Phi(c+2D,y,z)}{4} - \frac{D}{2}\left[\frac{\partial\Phi(x,y,z)}{\partial x}\right]_{x\,=\,c+2D} \tag{8}$$

where

$$\left[\frac{\partial\Phi(x,y,z)}{\partial x}\right]_{x\,=\,c+2D} = \sum_{lmn} \frac{l\pi}{\tilde{c}} A_{lmn} \cos\left[\frac{l\pi(c+2D)}{\tilde{c}}\right] \sin\left[\frac{m\pi y}{\tilde{a}}\right]$$

$$\sin\left[\frac{n\pi z}{\tilde{b}}\right]$$

and the emitted current from face 2 is

$$J_y^+ (x,a+2D,z) = \frac{\Phi(x,a+2D,z)}{4} - \frac{D}{2}\left[\frac{\partial\Phi(x,y,z)}{\partial y}\right]_{y = a+2D} \tag{9}$$

where

$$\left[\frac{\partial\Phi(x,y,z)}{\partial y}\right]_{y = a+2D} = \sum_{lmn} \frac{m\pi}{\tilde{a}} A_{lmn} \cos\left[\frac{m\pi(a+2D)}{\tilde{a}}\right] \sin\left[\frac{l\pi x}{\tilde{c}}\right] \sin\left[\frac{n\pi z}{\tilde{b}}\right]$$

B. The Scattered Flux

To use equation (4), with $\eta(\underline{r},\underline{r}'') = 0$, in calculating the uninterrupted scattered flux, $\Phi(x_o,y_o,z_o)$ at (x_o,y_o,z_o), it is necessary to define some angular dependence to the emitted current. Realizing it is difficult to make any generalization about the angular dependence of the emitted current, two possibilities for defining an angular dependence in terms of isotropy are:

1. Replace the emitting face with a plane semi-isotropic source (hereafter termed the semi-isotropic emitted current assumption) of strength $J^+(x,y,z)$ defined by equation (8) or (9).

2. Assume the current density, $\underline{j}(x,y,z,\underline{\Omega})$, is semi-isotropic (hereafter termed the semi-isotropic current density assumption) then

$$J^+ (x,y,z) = \int_{2\pi} \underline{n}\cdot\ \underline{j}(x,y,z,\underline{\Omega})d\underline{\Omega} \tag{10}$$

where $\underline{j}(x,y,z,\underline{\Omega}) = C\underline{\Omega}$ and $\underline{n}$ is the unit vector normal to the emitting area.

Based on the semi-isotropic emitted current assumption the angular emitted current from face 1, $K_{s1}(c+2D,y,z,\underline{\Omega})$, is

$$K_{s1}(c+2D,y,z,\underline{\Omega}) = \frac{J_x^+(c+2D,y,z)}{2\pi} \tag{11}$$

and the angular emitted current from face 2, $K_{s2}(x,a+2D,z\underline{\Omega})$, is

$$K_{s2}(x,a+2D,z,\underline{\Omega}) = \frac{J_y^+(x,a+2D,z)}{2\pi} \tag{12}$$

Based on the semi-isotropic current density assumption, the angular emitted current from face 1, $K_{s2}(c+2D,y,z,\underline{\Omega})$, is

$$K_{s1}(c+2D,y,z,\underline{\Omega}) = \underline{n}.\ \underline{j}(c+2D,y,z,\underline{\Omega}) = C_1 \cos\phi \tag{13}$$

where $\cos\phi = \underline{n}.\ \underline{\Omega}$ and ϕ is then the angle between the neutron direction and unit normal to the emitting face. Evaluation of equation (10) yields

$$C_1 = \frac{J_x^+(c+2D,y,z)}{\pi} \tag{14}$$

Similarly the angular emitted current from face 2, $K_{s2}(x,a+2D,z,\underline{\Omega})$, is

$$K_{s2}(x,a+2D,z,\underline{\Omega}) = \frac{J_y^+(x,a+2D_1z)}{\pi} \cos\phi \tag{15}$$

Using equation (4), with $\eta(\underline{r},\underline{r}'') = 0$, the uninterrupted flux, $\Phi(x_o,y_o,z_o)$ at (x_o,y_o,z_o), recalling that $2D<z_o<b+2D$, is determined for the two angular emitted currents as follows:

1. For the semi-isotropic emitted current assumption:

   a. If $2D<y_o<a+2D$ and $x_o>c+2D$ then only face 1 contributes to the flux at (x_o,y_o,z_o) and evaluation of equation (4) over $\underline{\Omega}$ and $\underline{\Omega}''$ yields

$$\Phi(x_o,y_o,z_o) = \int_{2D}^{a+2D}\int_{2D}^{b+2D} \frac{J_x^+(c+2D,y,z)dydz}{2\pi\left[\left[x_o-(c+2D)\right]^2+(y_o-y)^2+(z_o-z)^2\right]} \tag{16}$$

   b. Similarly, if $2D<x_o<c+2D$ and $y_o>a+2D$ then only face 2 contributes to the flux at (x_o,y_o,z_o) and

$$\Phi(x_o,y_o,z_o) = \int_{2D}^{c+2D}\int_{2D}^{b+2D} \frac{J_y^+(x,a+2D,z)dydz}{2\pi\left[(x_o-x)^2+\left[y_o-(a+2D)\right]^2+(z_o-z)^2\right]} \tag{17}$$

   c. If $y_o>a+2D$ and $x_o>c+2D$, then faces 1 and 2 contribute to the flux at (x_o,y_o,z_o) and

$$\Phi(x_o,y_o,z_o) = \text{equation (17)} + \text{equation (16)} \tag{18}$$

2. For the semi-isotropic current density assumption:

   a. If only face 1 contributes to the flux at (x_o,y_o,z_o) the evaluation of equations (4) over $\underline{\Omega}$ and $\underline{\Omega}''$ yields

$$\Phi(x_o,y_o,z_o) = \int_{2D}^{a+2D}\int_{2D}^{b+2D} \frac{\cos\phi_1 J_x^+(c+2D,y,z)\,dydz}{\pi\left[\left[x_o-(c+2D)\right]^2+(y_o-y)^2+(z_o-z)^2\right]} \tag{19}$$

where the integration of equation (4) over $\underline{\Omega}$ requires that

$$\cos\phi_1 = \cos\phi\left[\underline{\Omega}-\frac{\underline{r}''-\underline{r}}{|\underline{r}''-\underline{r}|}\right] = \frac{x_o-(c+2D)}{\left[\left[x_o-(c+2D)\right]^2+(y_o-y)^2+(z_o-z)^2\right]^{1/2}}$$

b. If only face 2 contributes to the flux at (x_o,y_o,z_o) then

$$\Phi(x_o,y_o,z_o) = \int_{2D}^{c+2D}\int_{2D}^{b+2D} \frac{\cos\phi_2 J_y^+(x,a+2D,z)\,dydz}{\pi\left[(x_o-x)^2+\left[y_o-(a+2D)\right]^2+(z_o-z)^2\right]} \tag{20}$$

where

$$\cos\phi_2 = \frac{y_o-(a+2D)}{\left[(x_o-x)^2+\left[y_o-(a+2D)\right]^2+(z_o-z)^2\right]^{1/2}}$$

c. If faces 1 and 2 contribute to the flux at (x_o,y_o,z_o) then

$$\Phi(x_o,y_o,z_o) = \text{equation (19)} + \text{equation (20)} \tag{21}$$

To evaluate the above integrals, a numerical technique is conveniently applied. The series in equations (8) and (9) are uniformly convergent so that the series can be integrated term by term. Thus each term in equations (16), (17), (19) and (20) can be integrated numerically

and a suitable convergence established. Results of scattered fluxes for a specific regular solid computed as outlined above are contained in the next section.

IV. METHOD OF MEASUREMENT AND CALCULATION

A. Method of Measurement

Measurements of the scattered flux were obtained with an arrangement simulating the geometry of Figure 2. As shown in Figure 3, a regular solid specimen, a polyethylene (C_2H_4) block (2.86 cm square x 5.16 cm long), was placed in a beam of thermal neutrons. A BF_3 detector was used to count scattered neutrons. The detector longitudinal axis remained perpendicular to face 2 and in the yz-plane at x = 1.43 cm + 2D, where D is the diffusion coefficient in cm. The center of the detector window was located at the following points (x_o, y_o, z_o) for measurement:

1. (1.43 cm + 2D, 7.86 cm + 2D, z_o) where z_o was incremented by by .5 cm from .5 cm + 2D to 4.5 cm + 2D.

2. Same as 1, except y_o = 12.86 cm + 2D.

The Pennsylvania State University TRIGA Reactor (Breazeale Nuclear Reactor Facility) provided the source neutrons. A D_2O tank between the beam port entrance and the reactor core provided sufficient thermalization such that the thermal flux at the beam port exit at a reactor power of 100KW was on the order of 10^7 neutrons per cm^2 per second. Collimation was achieved by placing in the beam port two iron plugs with 1-1/2 inch holes followed by a copper plug with a 3/4 inch hole. Smaller collimations would reduce background scattering, however, to maintain the specimen totally within the beam the above sizes were the minimum allowable. The specimen was placed 15 inches from the beam port exit and at this point, it was estimated that the beam had diverged

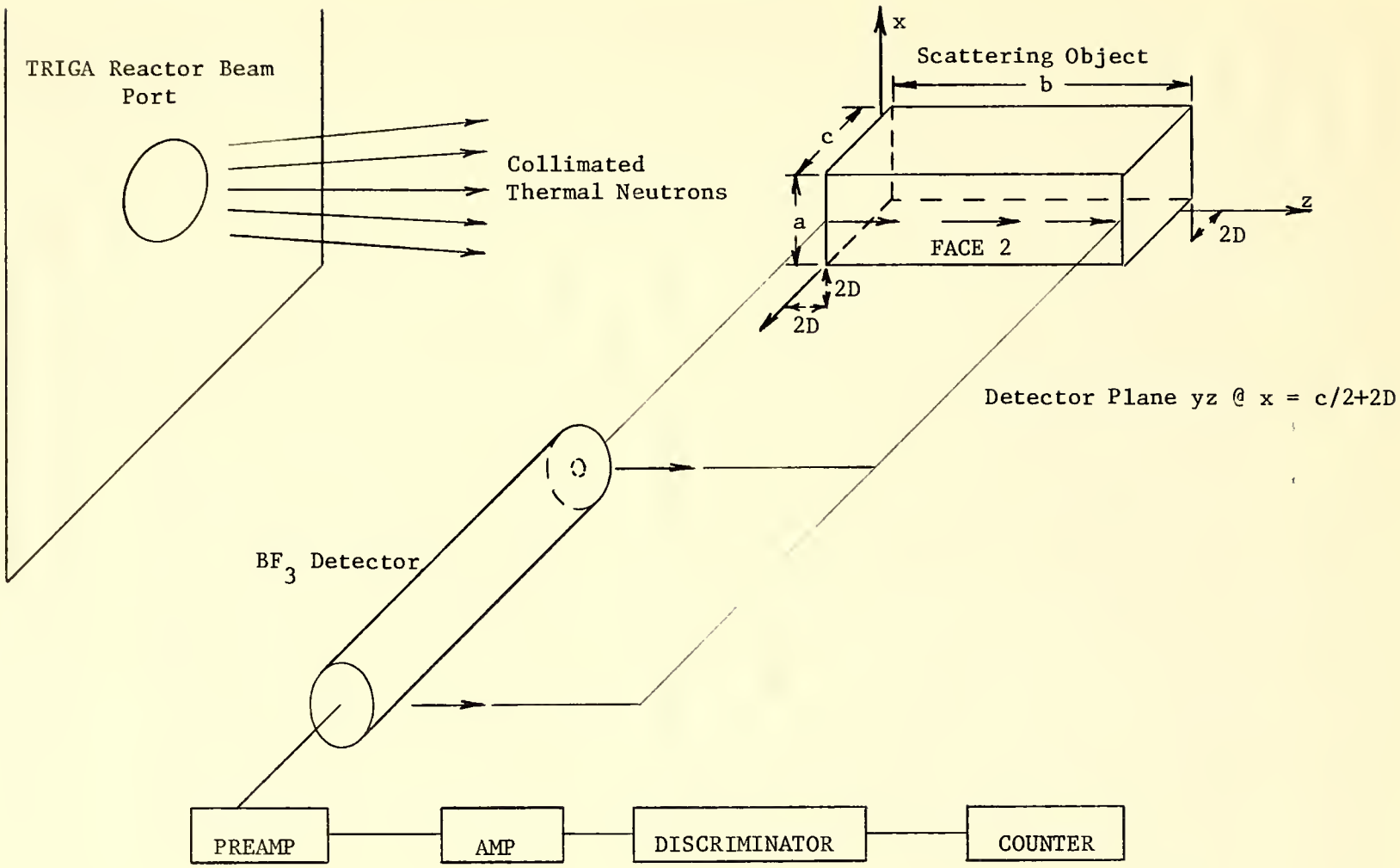

Figure 3. Diagram of Measurement Setup

to approximately twice the exit diameter with a flux on the order of 10^6 neutrons per cm^2 per second. The cadmium ratio in the beam was approximately 50.

The BF_3 detector was 14.5 inches long with a 1 inch outer diameter and was filled to a pressure of 60 cm Hg with BF_3 96% enriched in B^{10}. The detector was shielded with a cadmium jacket, and the window had a cadmium cover with a 1/16 inch diameter hole. By placing a neutron shutter between the beam port exit and the detector, an average signal to noise ratio of 2 was achieved. As shown in Figure 3 the neutron counting arrangement was typical for a gas filled proportional counter.

The polyethylene specimen was held in place by an aluminum clamp attached to a horizontal bar 1/4 inches in diameter. Three of the side faces were covered with a cadmium sheet which reduced background scatter from the aluminum holding stand, and maintained the integrity of the non-reentrant boundaries.

One minute background counts were taken at each point described above with only the specimen removed. The gross counts were also taken for one minute and were sufficiently high to yield counting fractional standard deviations on the order of .025. The counts obtained for points 5 cm (y_o = 7.86 cm + 2D) and 10 cm (y_o + 12.86 cm + 2D) from face 2 were normalized with the z_o - 2D = 2.5 cm point. The results are displayed on Figures 4 and 5. As discussed earlier, the normalized curve represents the relative scattered flux shape as amended by the detector response.

Additional measurements were made at 2.5 cm (y_o = 5.36 cm + 2D) from face 2. The measurements were repeated with various strips of cadmium on face 2 as follows:

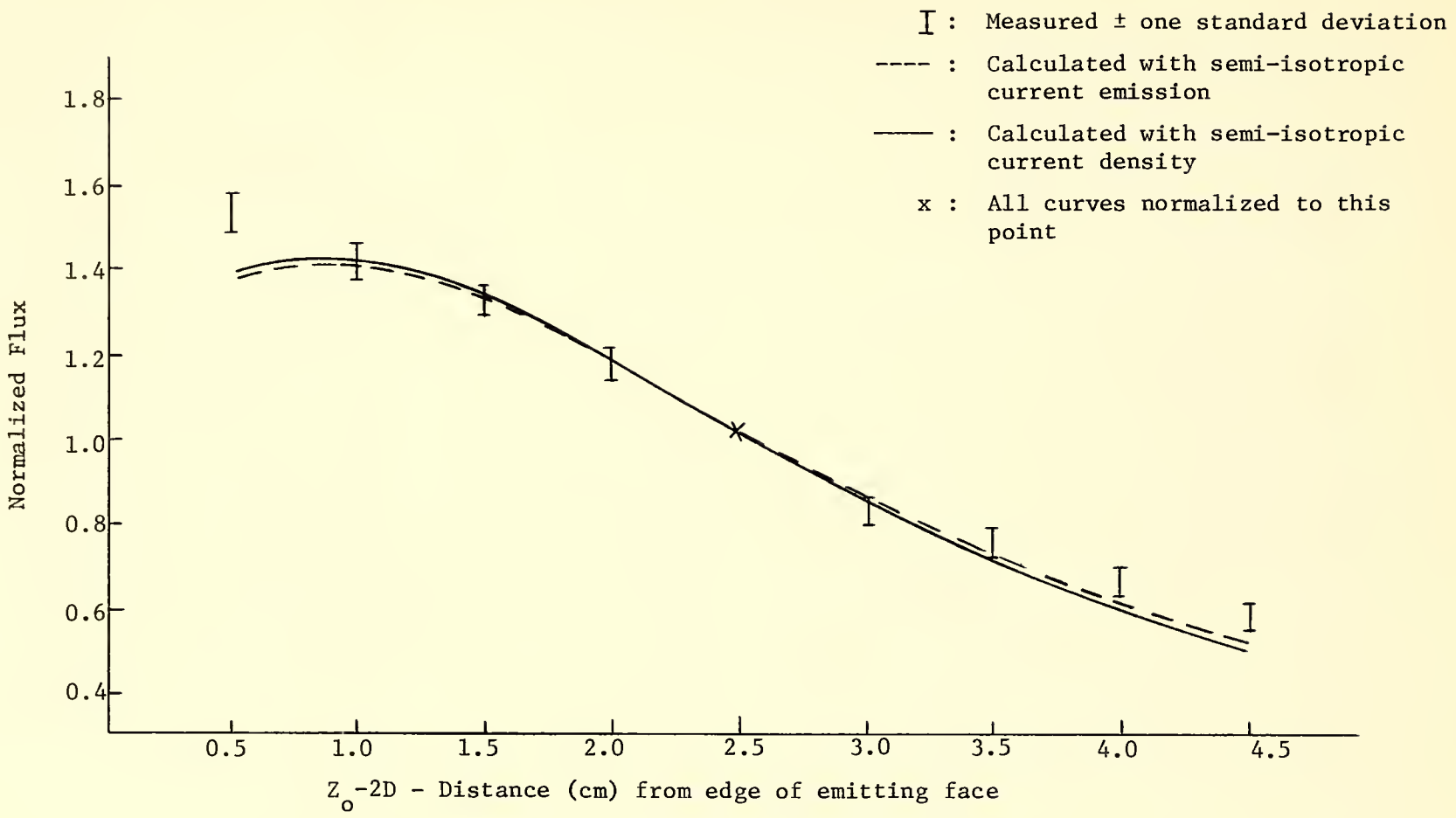

Figure 4. Calculated Flux Shape vs. Measured Flux Shape at Points (1.43cm±2D, 12.86cm±2D,z_o)

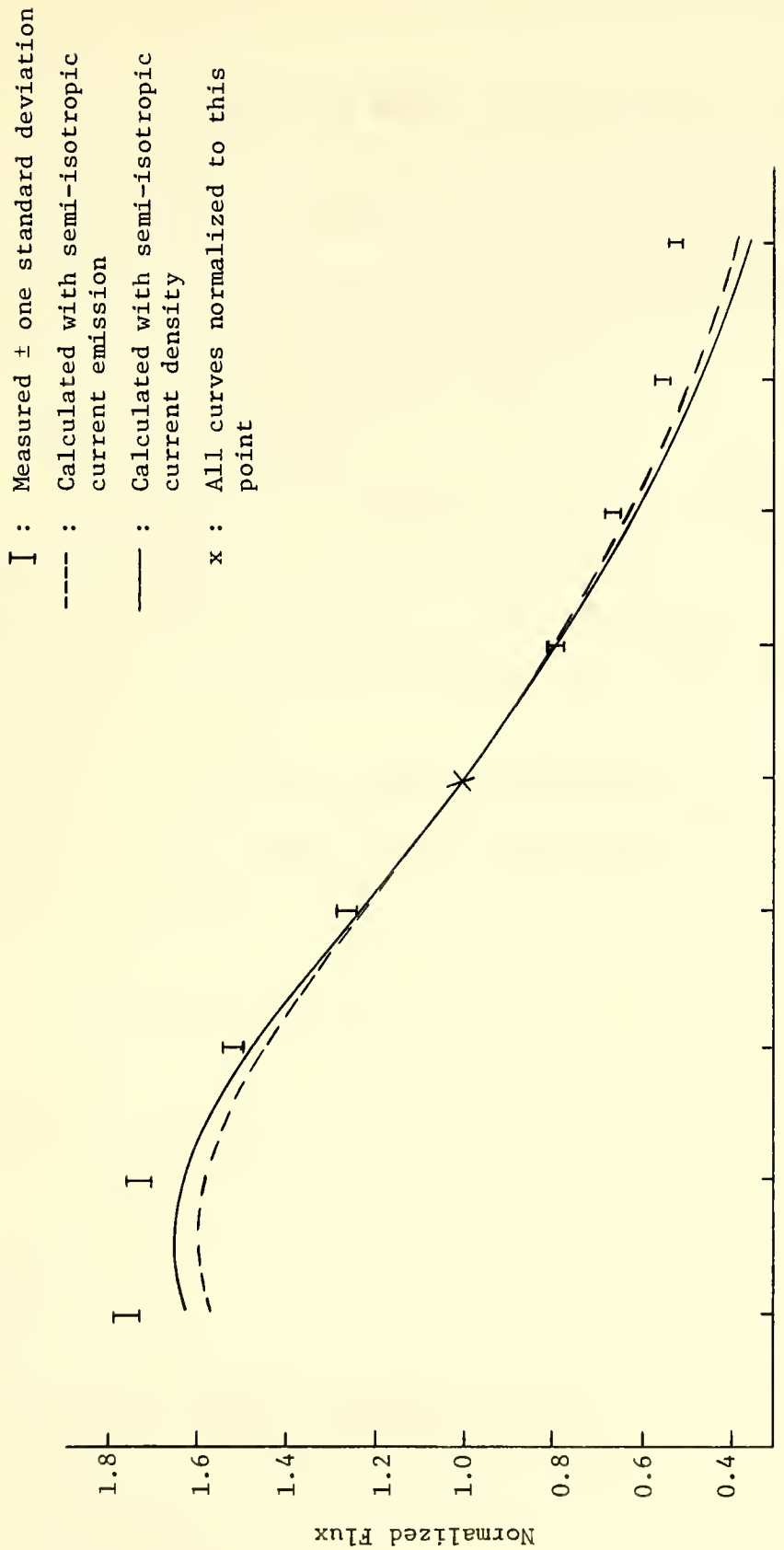

Figure 5. Calculated Flux Shape vs. Measured Flux Shape at Points (1.43cm±2D, 7.86cm±2D, z_o)

1. A 1 cm wide strip beginning at x = 1.5 cm + 2D and ending at x = 2.5 cm + 2D.

2. A 2 cm wide strip beginning at x = 1.5 cm + 2D and ending at x = 3.5 cm + 2D.

All counts obtained were normalized with count obtained at (1.43 cm + 2D, 5.36 cm + 2D, 2.5 cm + 2D). The results are displayed on Figures 6, 7, and 8.

B. Method of Calculation

The method of calculation was outlined in the previous section, and in this case equations (17) and (20) applied. To compare the calculations with the measured values, a response function was inserted representing the BF_3 detector response. The response function was determined as follows.

Neglecting the finite area of the detector face, the probability of detection for a neutron entering the detector at an angle θ with the detector face is

$$1 - \exp(-\bar{\Sigma}_t^B \, r/\cos\theta) \tag{22}$$

where $\bar{\Sigma}_t^B = \bar{\Sigma}_a^B$ is the thermal neutron absorption cross section of B^{10} at 60 cm Hg, r is the radius of the detector and $r/\cos\theta$ represents the path length of the neutron in the detector. For the geometry in Figure 3

$$\cos\theta = \left[\frac{(x_o-x)^2+(z_o-z)^2}{(x_o-x)^2+\left[y_o-(a+2D)\right]^2+(z_o-z)^2} \right]^{1/2} \tag{23}$$

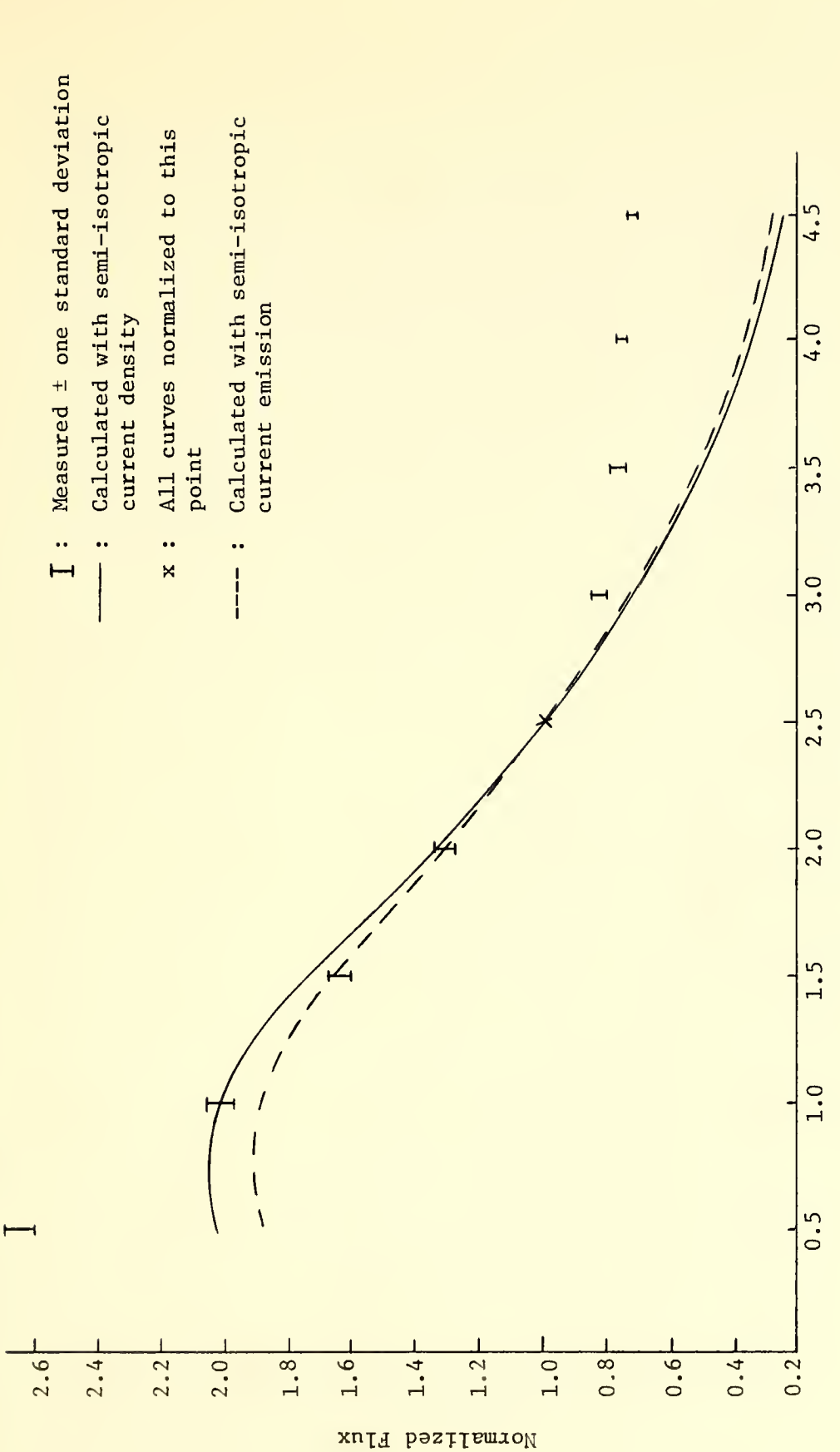

Figure 6. Calculated Flux Shape vs. Measured Flux Shape at Points (1.43cm+2D, 5.36cm+2D, z_o)

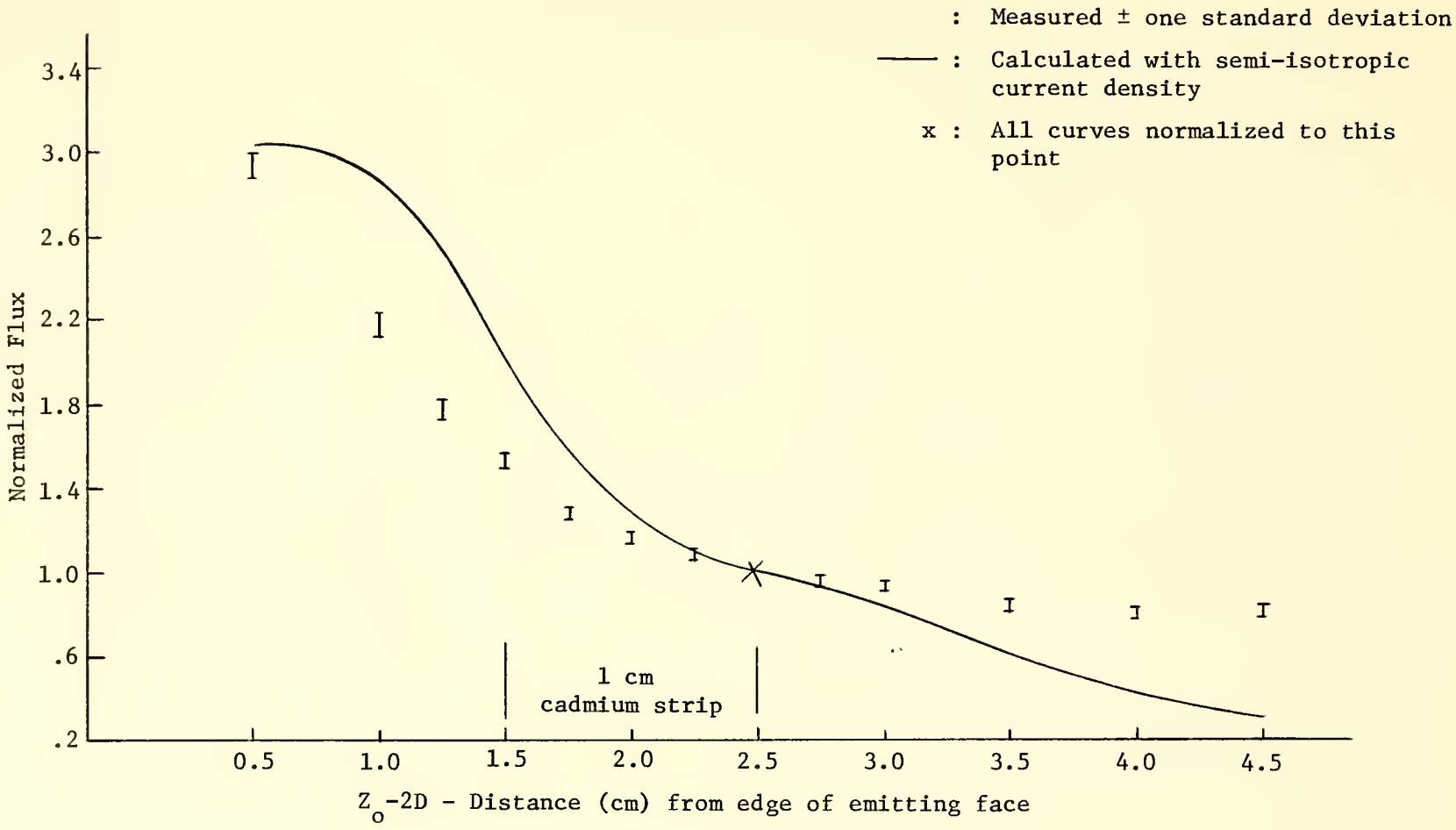

Figure 7. Calculated Flux Shape vs. Measured Flux at Points (1.43cm+2D, 5.36cm+2D,z_o) With a 1cm Cadmium Strip on Emitting Face

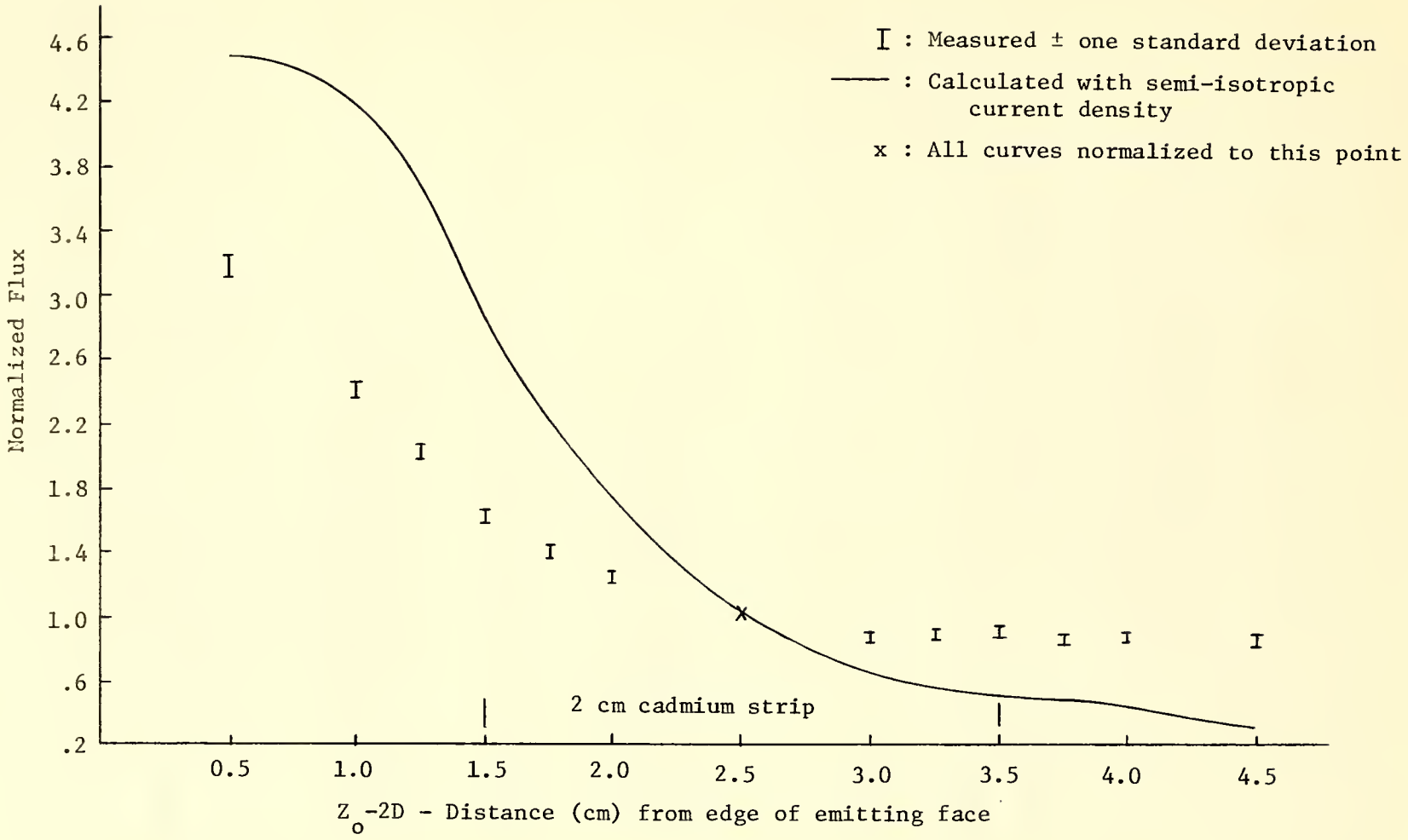

Figure 8. Calculated Flux Shape vs. Measured Flux at Points (1.43cm+2D, 5.36cm+2D,z_o) With a 2cm Cadmium Strip on Emitting Face

Considering the finite area of the detector window, a unit flux in the θ direction to the detector face produces a current of sin θ entering the detector, where from equation (23)

$$\sin\theta = \left[\frac{\left[y_o-(a+2D)\right]^2}{(x_o-x)^2+\left[y_o-(a+2D)\right]^2+(z_o-z)^2}\right]^{1/2} \tag{24}$$

The detector response function, $R(x_o,y_o,z_o,x,y,z)$, is then the fraction of the flux seen, equation (24), times the probability of detection, equation (22).

Assuming a semi-isotropic emitted current and accounting for the detector response, equation (17) was modified to

$$\Phi(x_o,y_o,z_o) = \int_{2D}^{c+2D}\int_{2D}^{b+2D} \frac{R(x_o,y_o,z_o,x,y,z)\ J_y^+(x,a+2D,z)dxdz}{2\pi\left[(x_o-x)^2+\left[y_o-(a+2D)\right]^2+(z_o-z)^2\right]} \tag{25}$$

Assuming a semi-isotropic current density equation (20) was modified to

$$\Phi(x_o,y_o,z_o) = \int_{2D}^{c+2D}\int_{2D}^{b+2D} \frac{R(x_o,y_o,z_o,x,y,z)\cos\theta_2\ J_y^+(x,a+2D,z)dxdz}{\pi\left[(x_o-x)^2+\left[y_o-(a+2D)\right]^2+(z_o-z)^2\right]} \tag{26}$$

Equations (25) and (26) were solved, as noted previously, by integrating each term numerically using as IBM system 370 Mod 168 computer and Argonne National Laboratory subroutine DROMB[10]. The series was truncated when the higher mode integral terms were less than .1% of the existing

sum. The thermal neutron diffusion properties of polyethylene were obtained from the ANL-5800[11]. Calculations were made for each point measured by the detector and were similarly normalized. The results for the semi-isotropic emitted current and for the semi-isotropic current density are displayed on Figures 4 and 5.

The calculations were repeated for the detector at 2.5 cm from face 2 as used in obtaining the measured values. Calculations were made at each point measured by the detector and were similarly normalized. Calculations with the cadmium strips on face 2 were made the semi-isotropic current density assumption only. The results are displayed on Figures 6, 7, and 8.

V. ANALYSIS OF RESULTS

In analyzing the results on Figures 4 through 8 it is helpful to bear in mind that:

1. The detector had a forward counting preference which decreased as the detector was moved away from the emitting surface (see equations (22) and (24)).

2. The emitted current, used in determining the angular emitted current, resulted from a diffusion calculation.

3. The angular emitted current was determined from assumptions regarding angular dependence.

As shown by Figure 4, at 10 cm from the emitting face the measured flux shape was generally well represented by the calculated flux shapes with differences only at points near the boundaries of the emitting face. Coupled with the detector forward counting preference, the boundary errors would be expected from a diffusion calculation. The differences, as displayed in Figure 4, indicate that the boundary errors were the result of calculated emitted currents which were low near the edges of the emitting face.

Additionally, a portion of the observed differences can be attributed to the assumptions used in defining an angular emitted current as the calculated flux shape for the semi-isotropic current emission differs from the calculated flux shape for the semi-isotropic current density emission. To quantitate somewhat, the maximum difference between the calculated relative flux for a semi-isotropic emitted current and the measured relative flux occurred at $z_o - 2D =$ 4.5 cm and was 15.1%. The difference between the calculated relative

flux for a semi-isotropic current density and the measured relative flux at the same point was 18.3%. Thus, the errors displayed by Figure 4 were due primarily to errors in the calculated emitted current near the boundaries.

As shown by Figure 5, when the detector was 5 cm from the emitting face, the boundary errors increased. This would be expected as the detector preference for points directly in front increased and the calculated emitted current was in error at the boundaries. Moreover, errors in the assumed angular dependence of the emitted current increased. To quantitate again at $z_o - 2D = 4.5$ cm, the difference between the calculated relative flux for a semi-isotropic emitted current and the measured relative flux was 26.8%. The difference between the calculated relative flux for a semi-isotropic current density and the measured relative flux was 33.8%.

As shown by Figure 6, when the detector was 2.5 cm from the emitting face, the differences increased further as would be expected. The differences in the calculated values for the semi-isotropic current density and the semi-isotropic current were small compared to the total errors. The principal source of the errors was again the calculated emitted current. Moreover, it should be noted that the block dimensions were only 1L x 2L, where L represents the diffusion length.

The measured and calculated flux shapes at 2.5 cm from the emitting face with 1 cm and 2 cm cadmium strips on the emitting face are displayed on Figures 7 and 8, respectively. The boundary errors displayed by Figure 6 are not as evident here, due to the normalization. In this case a significant portion of the face which had a reasonably

correct calculated emitted current was eliminated by the cadmium strip. As a result, the calculated flux at the $z_o - 2D = 2.5$ cm point had a larger contribution from the boundary areas yielding a low value. When normalized to this low value, the low values near the edges of the emitting face were dampened, decreasing the errors in the calculated relative flux.

The above comments can be summarized as follows. Differences between the calculated values and the measured values were due primarily to boundary errors in the calculated emitted current, with very minor effects due to the arbitrary assumptions used in defining the angular dependence to the emitted current. As the detector forward preference was decreased, the observed differences decreased and the calculated flux shapes represented well the measured values. Although large differences existed between the calculated and measured values when the detector had a strong forward preference, measured dips in the relative flux over a strong absorbing strip were represented by the calculated values.

VI. CONCLUSIONS

A. Summary

The diffusion approximation was applied in calculating emitted neutron currents from a homogeneous regular solid in a beam of thermal neutrons. The calculated emitted current, with an assumed angular dependence, was used in computing the scattered flux shape about the solid. Calculated results, modified for the response of a cylindrical gas filled proportional counter, were compared to values measured with a BF_3 proportional counter at points which received flux contributions from only one face of the solid. The observed differences in the calculated and measured flux shapes were due primarily to errors in the calculated emitted current about the edges of the face, with very minor effects due to the assumed angular dependence of the emitted current. As the directional preference of the detector decreased, the observed differences decreased. Moreover, regardless of a significant directional detector preference, trends in flux shapes over strong absorbing strips were well represented. It can be concluded that for a detector with a lesser directional preference, such as a film-converter detector, the calculated flux shape would better represent the measured flux and would be sufficient to complete the analytical representation.

B. Suggestions for Future Work

The description of the scattered neutron flux shape represents the first step in an analytical representation of the pseudo-hologram.

Future work is suggested to complete the analytical representation by including the response functions for the Fresnel zone plate previously described and for a typical film-converter detector. The detector response function will have to be suitably approximated as was done herein for the BF_3 detector response function. The flux shapes so determined could then be compared to calculated flux shapes based on an ideal detector and an ideal Fresnel zone plate in an effort to develop a correction factor for pseudo-holograms practically obtained. One possible application of a correction factor would be in correcting pseudo-holograms which are decoded numerically on a computer system[12]. The correction factor, depending on a general application, would at least decrease some of the resolution loss experienced in the real system.

APPENDIX

SOLUTION OF DIFFUSION EQUATION

The geometry is as shown in Figure 2. Then the extrapolated boundaries are

$$\tilde{c} = c + 4D$$

$$\tilde{a} = a + 4D$$

$$\tilde{b} = b + 4D$$

where c, a and b are the block dimensions.

The equation to be solved is

$$D\nabla^2\Phi(x,y,z) - \bar{\Sigma}_a\Phi(x,y,z) + S(x,y,z) = 0 \qquad \text{(A-1)}$$

where the source is

$$S(x,y,z) = \begin{cases} \bar{\Sigma}_s I_o e^{-\bar{\Sigma}_t(z-2D)} & \text{for } 2D<z<\tilde{b}-2D \\ 0 \quad \text{otherwise} \end{cases} \qquad \text{(A-2)}$$

and the boundary conditions are $\Phi(x,y,z)_{\substack{\text{extrapolated} \\ \text{boundary}}} = 0$ (A-3)

To solve (A-1) use

$$\nabla^2\phi(x,y,z) + B^2_{lmn}\phi(x,y,z) = 0 \qquad \text{(A-4)}$$

to generate a linear independent, complete, orthogonal set of functions $\{\phi_{lmn}(x,y,z)\}$ for $l,m,n = 1,2,3,\cdots$ where

$$\phi_{lmn} = \sin\left(\frac{l\pi x}{\tilde{c}}\right)\sin\left(\frac{m\pi y}{\tilde{a}}\right)\sin\left(\frac{n\pi z}{\tilde{b}}\right) \qquad \text{and} \tag{A-5}$$

$$B^2_{lmn} = \left(\frac{l\pi}{\tilde{c}}\right)^2 + \left(\frac{m\pi}{\tilde{a}}\right)^2 + \left(\frac{n\pi}{\tilde{b}}\right)^2 \tag{A-6}$$

Then

$$S(x,y,z) = \sum_{lmn} S_{lmn}\, \phi_{lmn}(x,y,z) \qquad \text{and} \tag{A-7}$$

$$\Phi(x,y,z) = \sum_{lmn} A_{lmn}\, \phi_{lmn}(x,y,z) \tag{A-8}$$

From the orthogonality property of $\{\phi_{lmn}(x,y,z)\}$ and equations (A-2) and (A-7), then

$$S_{lmn} = \frac{32\bar{\Sigma}_s I_o K}{\tilde{b}lm\pi^2\left[\Sigma_t^2 + \left(\frac{n\pi}{\tilde{b}}\right)^2\right]} \tag{A-9}$$

where

$$K = e^{-\bar{\Sigma}_t b}\left[-\bar{\Sigma}_t \sin\left[\frac{\pi n(\tilde{b}-2D)}{\tilde{b}}\right] - \frac{n\pi}{\tilde{b}}\cos\left[\frac{n\pi(\tilde{b}-2D)}{\tilde{b}}\right]\right] +$$

$$\bar{\Sigma}_t \sin\left(\frac{n\pi 2D}{\tilde{b}}\right) + \frac{n\pi}{\tilde{b}}\cos\left(\frac{n\pi 2D}{\tilde{b}}\right) \tag{A-10}$$

Substituting equations (A-7) and (A-8) into equation (A-1), using equation (A-4) and the linear independence of $\{\phi_{lmn}(x,y,z)\}$, then

$$A_{lmn} = \frac{S_{lmn}}{\bar{\Sigma}_a(1+L^2B^2_{lmn})} \tag{A-11}$$

where

$$L^2 = D/\bar{\Sigma}_a$$

Then using equations (A-8), (A-9), (A-10) and (A-11)

$$\Phi(x,y,z) = \sum_{lmn} A_{lmn}\, \phi_{lmn}(x,y,z) \qquad \text{(A-12)}$$

BIBLIOGRAPHY

1. Mertz, L. and N. O. Young. "Fresnel Transformation of Images." Proceedings of the International Conference on Optical Instrumentation, London, 305 (1961).

2. Barrett, H. H. "Fresnel Zone Plate Imaging in Nuclear Medicine." Journal of Nuclear Medicine, 13:382 (1972).

3. Barrett, H. H., P. T. Wilson and G. D. DeMeester. "The Use of Halftone Screens in Fresnel Zone Plate Imaging of Incoherent Sources." Optics Communications 5:398 (1972).

4. Barrett, H. H. and F. A. Harrigan. "Theory of Fresnel Zone Plate Imaging of Gamma Rays." Raytheon Technical Report T926. Submitted to Applied Optics.

5. Barrett, H. H. "Pulse Compression Techniques in Nuclear Medicine." Procedures IEEE, 60:723 (1972).

6. Rogers, W. L., K. S. Han, L. W. Jones and H. W. Beierwaltes. "Application of a Fresnel Zone Plate to Gamma Ray Imaging." Journal of Nuclear Medicine, 13:612 (1972).

7. Sider, R. G., E. S. Kenney and A. M. Jacobs. "Pseudo-Holography Using Scattered X-Rays." Nature, 249:546 (1974).

8. Rose, R. P. Personal Communication. The Pennsylvania State University, University Park, Pa. (1974).

9. Shulman, A. R. Optical Data Processing. Wiley, New York, p. 387 (1957).

10. Hielstrom, K. DROMB, OS/360 Fortran IV Routine for Two Dimensional Quadrature. Argonne National Laboratory, Argonne, Ill. (1966).

11. U.S. Atomic Energy Commission. ANL-5800, Reactor Physics Constants. U.S. Government Printing Office, Washington, D.C., 2nd ed. (1963).

12. Sider, R. G. "The Use of Coded Aperture Techniques in the Formation of Images with Scattered Penetrating Radiation." M.S. Thesis, The Pennsylvania State University, University Park, Pa. (1974).

Thesis
J548
157339
Johannesmeyer
A contribution to the study of imaging with scattered thermal neutrons.